

Independent Control of Copolarized Amplitude and Phase Responses via Anisotropic Metasurfaces

Rui Yuan Wu, Lei Bao, Liang Wei Wu, Zheng Xing Wang, Qian Ma, Jun Wei Wu, Guo Dong Bai, Vincenzo Galdi,* and Tie Jun Cui*

A class of anisotropic, transmissive electromagnetic metasurfaces is presented, which enable independent and simultaneous control of copolarized phase and amplitude responses to two linear, orthogonal polarizations. By varying the geometrical parameters, the transmission response of the proposed structure can yield a full phase coverage, accompanied by broadly adjustable amplitude and negligible cross-polarized components. The full amplitude-phase control together with the novel anisotropic character allows efficient implementation of complicated field manipulations. As representative application examples, which cannot be realized via conventional (phase-only) metasurfaces, it is presented here: (1) the radiation of multiple equal-power vortex beams (along arbitrarily predesigned directions, with designable orbital angular momentum modes under different polarizations), and (2) the realization of polarization-reconfigurable multifocal metalenses. Full-wave numerical simulations and experimental results demonstrate good agreement and confirm the versatility and effectiveness of the proposed approach to design advanced field-manipulation systems.


Metasurfaces are ultrathin artificially engineered structures that can be viewed as the 2D versions of volumetric metamaterials. They are generally composed of periodic or aperiodic arrangements of artificial subwavelength meta-atoms, and provide a powerful and versatile tool for manipulating electromagnetic (EM) waves,^[1,2] while maintaining low profile and lightweight characteristics, as well as ease of fabrication. In the wake of the early work by Sievenpiper et al.^[3] on mushroom-shaped bandgap structures, powerful modeling tools such as the generalized sheet transition condition^[4] and transverse resonance method^[5] have been proposed to analyze the EM response of metasurfaces. In 2011, Yu et al.^[6] introduced a novel theory

of generalized Snell's laws, wherein the shape and direction of a wavefront are controlled via an artificial phase distribution imparted by a metasurface, essentially relying on a resonance mechanism and polarization conversion. This groundbreaking study has triggered a surge of interest in this research area, with the proposal of several working mechanisms, including reflection,^[7,8] transmission,^[9–11] and surface-wave types.^[12,13] Besides these common metallic structures with dielectric substrates, also worth of mention are all-dielectric^[14,15] and all-metallic alternatives.^[16,17] The availability of broad libraries of meta-atom responses, together with the generalized Snell's laws, provides an effective design tool to manipulate EM wavefronts in a powerful and versatile fashion by only considering the scattering responses and desired amplitude or phase distributions on the metasurface equivalent aperture. The reader can refer to refs.[18–20] for discussions of the limitations of the underlying approximations and more rigorous approaches. Recently, “digital coding” and “programmable” metasurfaces have also emerged as a fascinating paradigm due not only to their capabilities of digitally manipulating EM waves, but also to the profound implications from the perspective of information science.^[21]

As previously mentioned, metasurfaces have demonstrated great potential in manipulating the reflection or transmission phase in a somehow easier and more effective fashion than volumetric metamaterials, finding many interesting applications from microwaves to optical wavelengths, including absorbers,^[7,22] polarization manipulations,^[23,24] focusing,^[25,26] and holograms.^[27–29] However, metamaterials inherently offer more degrees of freedom and systematic design procedures (e.g., ray-tracing and transformation optics^[30,31]) to fully tailor the wavefronts, which have no counterpart for metasurfaces due to their very working principles. In fact, if amplitude and phase responses could be controlled independently, metasurfaces would also be able to synthesize arbitrary wavefront shapes and propagation directions. However, designing meta-atoms with such characteristics is a grand challenge since manipulations of both amplitude and phase responses rely on resonances, which inherently induce mutual interferences. Within this framework, there has been an intense research effort to overcome these difficulties, and several amplitude–phase (*A–P*) controllable designs have been put forward. In 2014, Liu et al.^[32]

Dr. R. Y. Wu, Dr. L. Bao, Dr. L. W. Wu, Dr. Z. X. Wang, Dr. Q. Ma, Dr. J. W. Wu, Dr. G. D. Bai, Prof. T. J. Cui
State Key Laboratory of Millimeter Waves
Southeast University
Nanjing 210096, China
E-mail: tjcui@seu.edu.cn

Prof. V. Galdi
Fields & Waves Lab
Department of Engineering
University of Sannio
Benevento I-82100, Italy
E-mail: vgaldi@unisannio.it

 The ORCID identification number(s) for the author(s) of this article can be found under <https://doi.org/10.1002/adom.201902126>.

DOI: 10.1002/adom.201902126

proposed a C-shaped structure to control the amplitude and phase responses of cross-polarized wavefronts by adjusting the opening and orientation angles. This work introduced a key idea to design *A–P* controllable metasurfaces within the terahertz and microwave bands, by considering the cross-polarized response in view of its broader operational bandwidth, relatively simple design procedure, and weaker interactions between the amplitude and phase responses, thereby paving the way to a series of interesting applications.^[33–36] However, this working mechanism does not enable an anisotropic response, i.e., independent control of the responses to two linear, orthogonal polarizations. Subsequent studies have demonstrated the possibility to control copolarized amplitude and phase responses by relying on indium tin oxide-based^[37] and Huygens^[38] metasurfaces, but with inherent restrictions in the attainable amplitude range, or the operability limited to a single polarization.

Against the above background, we propose here an anisotropic metasurface platform that is capable to fully and independently control the copolarized amplitude and phase responses to two linear, orthogonal polarizations, thereby addressing the challenges above. The proposed structure relies on an anisotropic meta-atom composed of tightly stacked cross-shaped patches and slots. By varying their sizes, a full 2π phase excursion can be obtained in the copolarized transmission response, with amplitude adjustable from 0 to 0.9, simultaneously and independently for *x*- and *y*-polarized fields. This enables the synthesis of advanced functionalities, via predesigned

amplitude and phase patterns, which can be controlled by the incident polarization state.

From the application viewpoint, a typical scenario of interest for the above-mentioned *A–P* controllable metasurfaces is a shared-aperture antenna with multibeam radiation patterns. We also highlight that the proposed structure yields a potentially broadband response as the operational frequency can be adjusted by only changing the variation range of the size parameters with a fixed periodic spacing of the meta-atoms. To the best of our knowledge, this represents the first evidence of a fully anisotropic control of the copolarized transmission amplitude and phase responses, thereby providing new degrees of freedom by comparison with the existing isotropic *A–P* controllable metasurfaces. The outcomes of our study, validated via both numerical simulations and experiments, set the stage for advanced applications in multifunctional and multitarget radar and communication systems.

Figure 1a schematically illustrates the working principle of the proposed anisotropic *A–P* controllable metasurface. For *x*- and *y*-polarized EM plane waves impinging on the metasurface, the transmitted amplitudes and phases can be controlled independently and simultaneously by suitably varying the geometrical parameters of the meta-atoms. As it will be clearer in the examples discussed hereafter, this enables advanced wavefront manipulations.

The meta-atom geometry, illustrated in **Figure 1b–d**, comprises a stack of metallic cross-shaped patches and slot

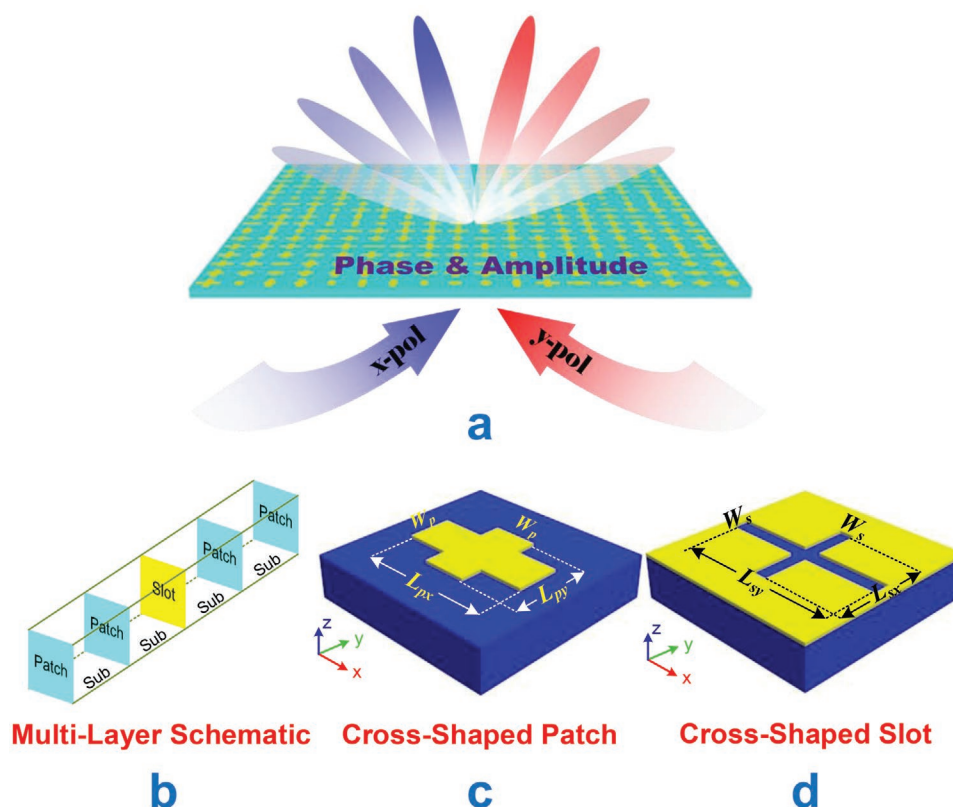


Figure 1. a) Conceptual illustration of the proposed anisotropic metasurface. The amplitude and phase responses in transmission for both *x*- and *y*-polarized EM fields can be controlled independently and simultaneously, thereby enabling full control of the copolarized responses. b) Schematic of the multilayer meta-atom; c, d) geometries of the cross-shaped patch and slot, respectively.

elements laid on dielectric substrates. Specifically, it includes four identical cross-shaped patches composed of two orthogonal copper strips, with fixed widths $W_p = 2$ mm and variable lengths L_{px} and L_{py} . The cross-shaped slot has a complementary pattern, likewise with fixed width $W_s = 0.5$ mm and variable lengths L_{sx} and L_{sy} . The substrates are 1.5-mm-thick and made of F4B, with relative permittivity $\epsilon_r = 3.5$ and loss tangent $\tan \delta = 0.003$. Due to the resonant mechanism, the horizontal (vertical) strips of the patch and the vertical (horizontal) slot arms are sensitive to x -polarized (y -polarized) EM waves. Cross-shaped structures exhibit good anisotropic properties since the size changes in one direction have little influence on the sizes in the other direction, which minimizes the mutual interference between the two polarizations. As a result, we can control independently and simultaneously the copolarized transmission responses to x - and y -polarized fields by varying L_{px}, L_{py} , and L_{sx}, L_{sy} , respectively. In view of the inherent symmetry of the structure, it is sufficient to illustrate the working principle for one polarization only; in what follows, we focus on the manipulation of x -polarized EM fields.

Figure 2b,e shows the transmission-coefficient copolarized amplitude and phase distributions at 11 GHz as a function of the geometrical parameters L_{px} (from 2 to 7.5 mm) and L_{sx} (from 0.5 to 8.9 mm), by assuming a meta-atom period of 9 mm. Here and henceforth, an implicit $\exp(j2\pi ft)$ time-harmonic

dependence is assumed, with f denoting the operational frequency. We observe that the armlengths of the patches and slot essentially control the phase and amplitude responses, respectively. Although the relationships are complicated and nonlinear, from the dynamic ranges observable in Figure 2b,e, it is apparent that an arbitrary A - P combination can be in principle attained via a suitable choice of L_{px} and L_{sx} , thereby demonstrating the anticipated full control. Table 1 summarizes some details of the typical designs available in the topical literature, and compares them with the proposed approach.

As can be expected, the meta-atom period should be proportional to the operational wavelength in order to excite the necessary resonance phenomenon. This implies some inherent restrictions in the operational frequency once the period is fixed. Existing studies on A - P controllable metasurfaces^[37,38] show that it is challenging to achieve broadband or multiband performance in copolarized schemes in view of the inherent narrow-band character of the resonance. Interestingly, as illustrated in Figure 2a,d–f, our proposed meta-atom can also work at 10 and 12 GHz, by changing the range of L_{px} to 2–8 and 2–7 mm, respectively, without varying the period. In fact, the proposed design maintains excellent A - P control capabilities within the frequency range 9.5–12.5 GHz by suitably selecting the variation range of L_{px} . Although this somehow differs from the traditional broadband concept, we think it can

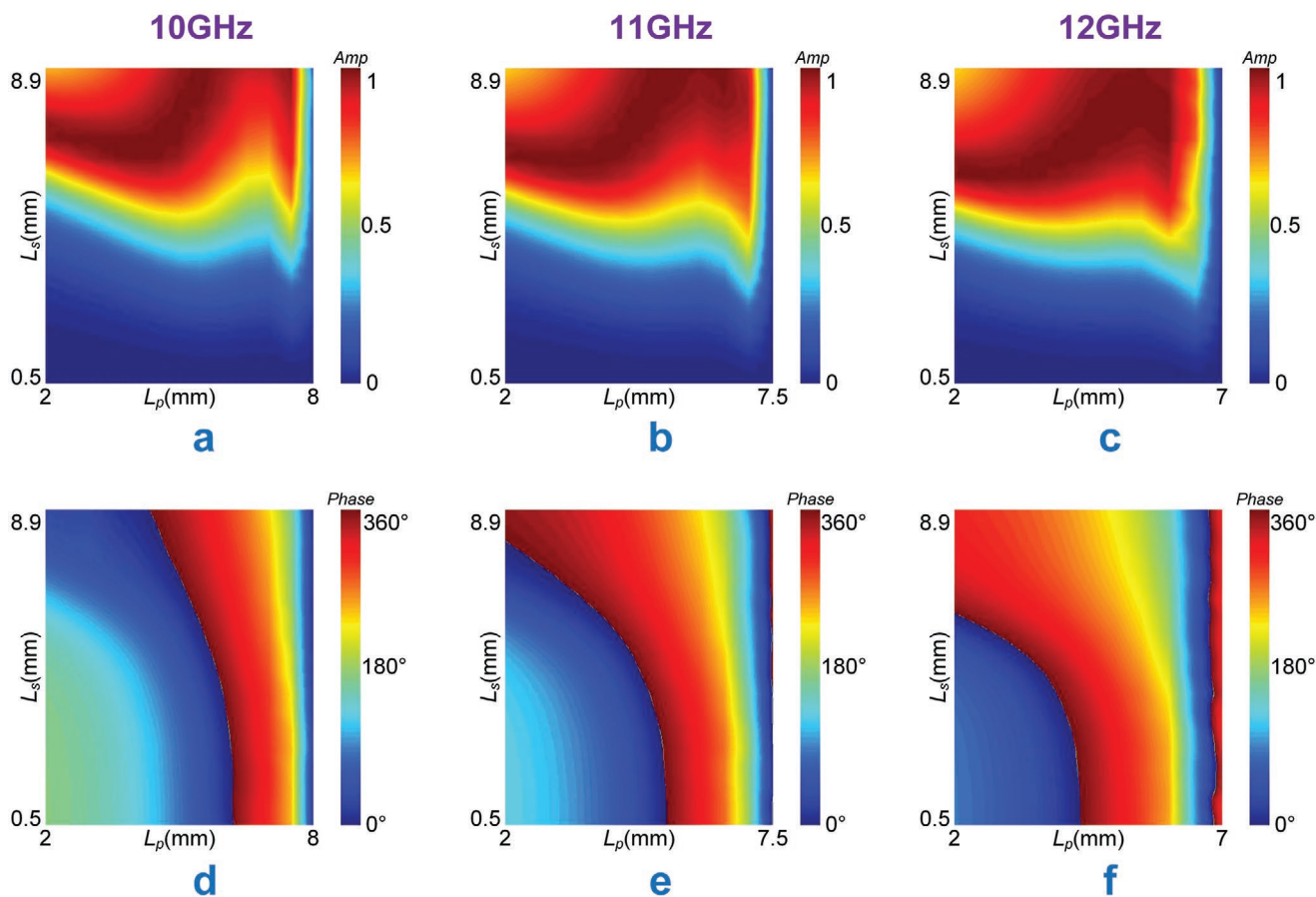


Figure 2. Copolarized transmission-coefficient responses for a meta-atom period of 9 mm, as a function of the parameters L_p (L_{px} or L_{py}) and L_s (L_{sx} or L_{sy}), at different frequencies. a–c) Amplitude and d–f) phase responses at 10, 11, and 12 GHz, respectively.

Table 1. Details of several typical A – P controllable metasurfaces.

Study	Amplitude	Phase range	Polarization
Ref. [32]	Cross-Polarization Range: 0–1	2π	Independent
Ref. [33]	Cross-Polarization Range: 0–1	2π	Independent
Ref. [34]	Cross-Polarization Range: 0–1	2π	Independent
Ref. [37]	Copolarization Range: 0.3–0.7	2-bit	Independent
Ref. [38]	Copolarization Range: 0–0.85	2π	x-polarization
This work	Copolarization Range: 0–0.9	2π	Anisotropic

also be regarded as an unconventional broadband property. Interestingly, this enables in principle to realize broadband programmable metasurfaces via the integration of active devices such as diodes.^[21]

To gain some insight in the working mechanism of our proposed meta-atom, we recall that a similar multilayer geometry (with square-shaped patches and horizontal slots) was previously proposed^[39] to realize full-space manipulations. In such structure, the x -directed slot allows the transmission of y -polarized EM fields, while reflecting back x -polarized ones. Therefore, the slot length can be utilized to control the transmitted amplitude. This concept was also exploited in another study,^[40] in which a dual-band transmitarray was realized by etching several slots of different lengths. Specifically, it was shown that the slot layer acts as a frequency-selective structure, in which the operational frequency can be tuned by acting on the slot length. The working mechanism can be summarized in terms of three conditions: (1) electrical resonances occur in the slot; (2) the working frequency depends on the length of the slot; (3) the transmitted amplitude depends on the resonance strength, which peaks at the resonant frequency and decreases when the frequency shifts. Therefore, we can conclude that the transmitted amplitude can be manipulated by acting the slot length. This mechanism is quantitatively illustrated in Figure S1 in the Supporting Information. Although this phenomenon also affects the phase response, the induced variations can be compensated by the extra phase shift provided by the patch layers. Since slots of various lengths can yield resonances at different frequencies, and the patches also exhibit intrinsic broadband properties, our proposed structure can work at multiple frequencies by properly selecting the size ranges. To sum up, a carefully engineered combination of patch- and slot-type layers enables independent and simultaneous control of the copolarized amplitude and phase transmission responses, which also possibly enables the dynamical manipulation of the amplitude and phase responses by exploiting active devices (instead of geometrical variations) to chance the resonance response.

From the application viewpoint, a typical scenario of interest for the above-mentioned A – P controllable metasurfaces is a shared-aperture antenna with multibeam radiation patterns. Although in most cases the attention is focused on pencil beams,^[36,41,42] vortex beams are eliciting a growing attention.

However, available studies on this subject^[15,39,43,44] rely on the tailoring of the phase-response only, with separation mechanisms based on the working polarization or space, which do not really yield a true superposition of multimode vortex beams. More important, the beam powers radiated in different directions (with same or different orbital angular momentum (OAM) modes) cannot be controlled. These inherent limitations stem from the lack of control in the amplitude response. Another important application scenario of A – P control is the design of multifocal metalenses, which is very hard to realize with phase-only metasurfaces and typically requires computationally intensive optimization algorithms. Within this framework, available designs include both reflection- and transmission-types as well as dual-frequency operation.^[33,34,45,46] However, the polarization state has not hitherto been exploited to reconfigure the focusing functionality in view of the inherent difficulty in achieving A – P control with anisotropic characteristics. Aimed to solve these problems, we will take advantages of our proposed A – P controllable to construct the synthesis of multiple equal-power vortex-beam radiation patterns and polarization-reconfigurable multifocal metalenses.

Shared-aperture multi-beam radiation represents one of the most interesting applications of metasurface-based antennas. The most common approach relies on the superposition of several basic amplitude and phase pattern as follows

$$E_f(m, n) = a_f(m, n) \exp[j\varphi_f(m, n)] = \sum_{b=1}^T E_b(m, n) = \sum_{b=1}^T a_b(m, n) \exp[j\varphi_b(m, n)] \quad (1)$$

where $a(m, n)$ and $\varphi(m, n)$ denote the amplitude and phase of the (m, n) -th meta-atom on the aperture, respectively, and the subscripts f and b indicate the final and basic patterns, respectively. As already mentioned, phase-only metasurfaces allow partial control of the degrees of freedom, whereas our proposed A – P control grants access to the entire effective information contained in every basic pattern. Among other things, this also enables power manipulations of the radiated beams. In view of the relationship between the transmitted amplitude and final radiated power, it is expedient to define a power-controlling parameter $p = a_f^2(m, n)$. Following ref. [42] and more detailed derivations in the Supporting Information, for varying angles of deflection, the power controlling parameter p should be adjusted as

$$\frac{\cos^2 \theta_j}{\cos^2 \theta_i} = \frac{p_i}{p_j} \quad (2)$$

with the subscripts i, j indicating two possible directions. Therefore, it is possible to manipulate the power of all the beams radiated along different directions in a flexible fashion. The relationship above can also be extended so as to control multiple vortex beams, which has never been achieved in previous studies.

Due to the anisotropic characteristics of the meta-atom, it is possible to synthesize two different multiple-beam radiation functionalities on the same aperture, so that equal-power vortex beams with designable OAM modes are radiated along arbitrarily predesigned directions. Specifically, we exploit the concept of

coding metasurfaces^[21] to synthesize the deflecting patterns by designing suitable 1D coding sequences. The design procedure is similar to that in ref. [39]: By means of convolution operations,^[47] the phase compensating pattern (converting the spherical incidence to a plane wave), the deflecting pattern and the functional OAM pattern are integrated together in a coding metasurface to attain a basic deflecting vortex beam. The final coding pattern is obtained by the superposition of these multiple basic patterns.

As a first example, we synthesize three x -polarized equal-power vortex beams with same OAM mode radiated simultaneously along different directions in the x - z plane. The OAM pattern here is chosen as the mode 0, i.e., a conventional pencil beam. The design procedure is illustrated in Figure S2 in the Supplementary Information, where the deflecting patterns are encoded by the 2-bit sequences S1(00000000...), S2(33221100...), and S3(01230123...), respectively. Here, and henceforth, the coding states “0,” “1,” “2,” and “3” correspond to phases of 0°, 90°, 180°, and 270°, respectively. The deflection angles can be calculated as^[21]

$$\theta = \arcsin\left(\frac{\lambda}{\Gamma}\right) \quad (3)$$

where λ is the wavelength at the working frequency of 11 GHz, and Γ is the period of the coding sequence. Accordingly, the calculated deflection angles are $\theta_1 = 0$, $\theta_2 = -22.3^\circ$, and $\theta_3 = 49.2^\circ$. From Equation (2), and taking into account the maximum achievable transmission, the amplitude values of the three patterns are chosen as 0.5868, 0.6345, and 0.9. After the convolution operations, three basic patterns are superposed via Equation (1), yielding the final amplitude and phase distributions shown in Figure 3a.

For the y -polarized case, we address a more challenging design, which involves different OAM modes. Specifically, we select for the three radiated beams the OAM modal orders 0, +1, and -1. For the 0-mode pattern, the phase distribution stays constant on the aperture, whereas for the +1 and -1 modes, 0°–360° spiral phase distributions (anticlockwise and clockwise, respectively) are synthesized. The same deflecting-pattern coding sequences are utilized as for the x -polarized case. It should be highlighted that Equation (2) only applies to pencil beams, and hence it cannot be applied in this case. Accordingly, the amplitude values of the three beams are numerically optimized to 0.36, 0.639, and 0.9. The entire process is illustrated in Figure S3 in the Supporting Information, and the final amplitude and phase distributions are shown in Figure 3b. All the design details, for both polarizations, are summarized in Table 2.

To validate the proposed design, we carry out both full-wave simulations and measurements. The metasurface is composed of 24×24 meta-atoms and occupies an area of 216×216 mm². A photograph of the prototype is shown in Figure 3c. We first measure the far-field radiated patterns in a microwave chamber, as illustrated in Figure S4 in the Supporting Information. Figure 3d compares the simulated and measured x -polarized far-field radiation patterns, showing a very good agreement. We observe that, in line with the specifications, the three pencil beams have their peaks at -22.3° , 0° , and $+49.2^\circ$, and exhibit equal power levels. Figure 3e

shows the corresponding results for the y -polarized case. Once again, simulations and measurement are in good agreement, with the 0-mode (pencil beam) peaked at 0° , the nulls of the vortex beams with +1 and -1 modes observed at -22.3° and $+49.2^\circ$, and the three beams exhibiting very similar powers, in line with the specifications. To further illustrate the vortex-beam characteristics, we also carry out near-field simulations and measurements (at a plane located about 300 mm from the sample) as illustrated in Figure S5 in the Supporting Information. In Figure 3f, the upper four panels show the simulated intensity and phase distributions of the OAM +1 and -1 modes, respectively, whereas the lower panels show the corresponding measured results. We observe the expected center-null intensity profiles and spiral-phase profiles, in fair agreement between simulations and measurements, thereby demonstrating that multiple equal-power vortex beams with same or different OAM modes are successfully integrated on the same aperture without mutual interference.

A metalens essentially converts a planar EM wavefront into a focusing distribution at a predesigned focal plane. Whereas a single focus can be easily obtained via conventional phase-only metasurfaces, multifocusing responses require complicated optimization algorithms. Instead, by enabling amplitude control, multifocusing responses can be superposed directly. Here, we consider the two basic schemes, i.e., axial and lateral bifocal metalenses, to demonstrate arbitrary dual-focusing responses. More complicated bifocal metalenses can be regarded as the combination of these basic properties. In our proposed platform, the two schemes are integrated in a single metasurface, and can be reconfigured by changing the polarization thanks to the inherent anisotropy. This yields unprecedented polarization-reconfigurable properties.

The complex-valued transmission-coefficient distributions of 1D anisotropic axial and lateral bifocal metalenses should satisfy the following conditions

$$T(x) = A_1 \exp\left[jk\left(\sqrt{x^2 + F_1^2} - F_1\right)\right] + A_2 \exp\left[jk\left(\sqrt{x^2 + F_2^2} - F_2\right)\right] \quad (4)$$

$$T(y) = A_1 \exp\left[jk\left(\sqrt{(y+d_1)^2 + F^2} - F\right)\right] + A_2 \exp\left[jk\left(\sqrt{(y+d_2)^2 + F^2} - F\right)\right] \quad (5)$$

where $A_{1,2}$ is the focus amplitude (chosen as $A_1 = A_2 = 1$ in the examples below), $k = 2\pi/\lambda$ is the free-space wavenumber, $d_{1,2}$ is the offset distance from the central axis (with positive and negative values denoting right and left shifts from the central axis, respectively), and $F_{1,2}$ is the focal length, with the subscripts 1 and 2 indicating the axial and lateral configuration, respectively. Similar to what already discussed in connection with multibeam radiation, these conditions are actually the superposition of two basic single-focus metalens patterns.

It is also possible to synthesize 2D anisotropic bifocal metalenses by considering the x - and y -directions simultaneously. Accordingly, Equations (4) and (5) are extended to a 2D scenario as follows

$$T(x, y) = A_1 \exp\left[jk\left(\sqrt{x^2 + y^2 + F_1^2} - F_1\right)\right] + A_2 \exp\left[jk\left(\sqrt{x^2 + y^2 + F_2^2} - F_2\right)\right] \quad (6)$$

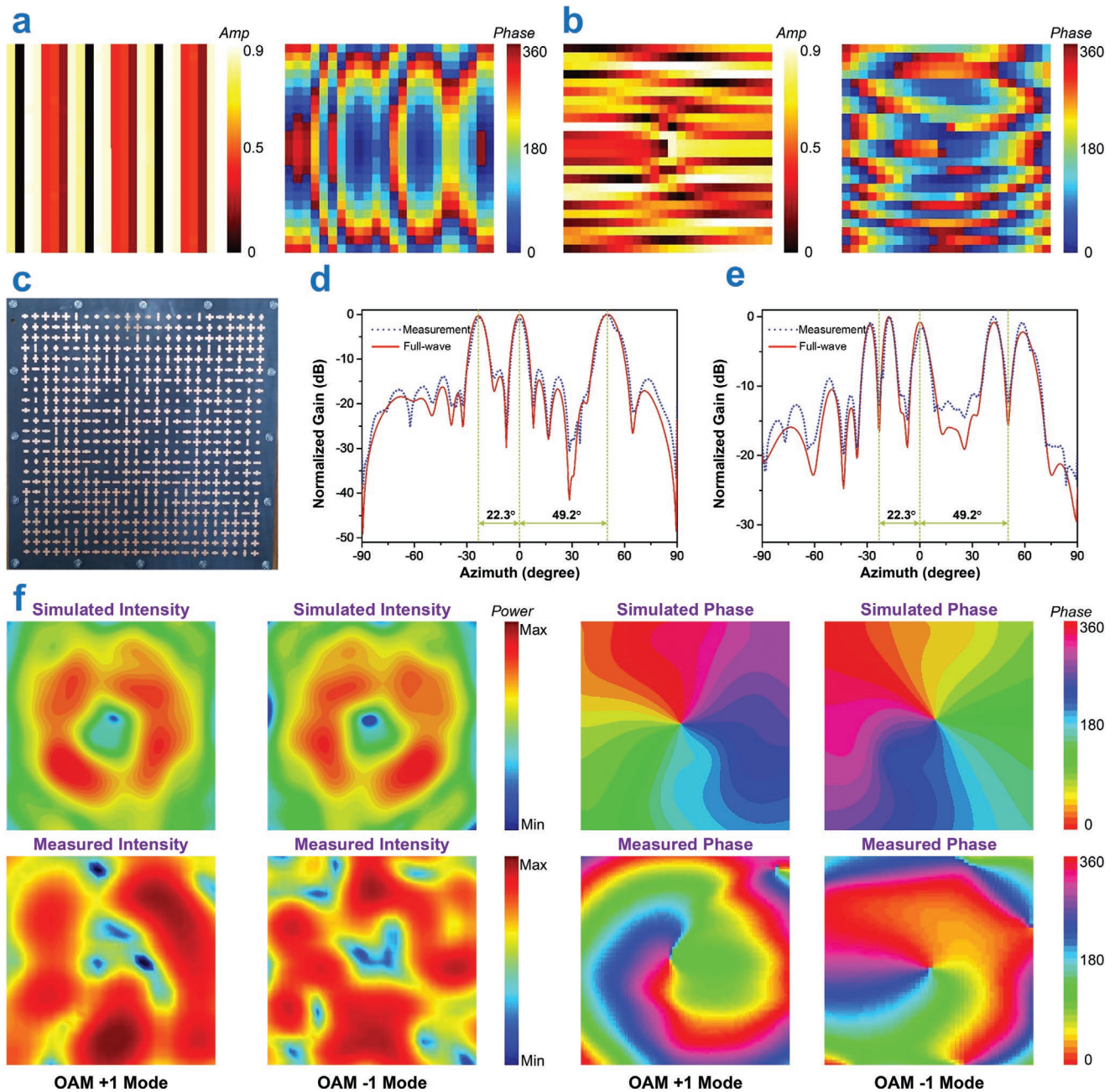


Figure 3. a) Amplitude and phase distributions for the three x-polarized equal-power vortex beams (all modes 0). b) Amplitude and phase distributions for the three y-polarized equal-power vortex beams (−1, 0, and +1 modes). c) Photograph of the fabricated prototype. d) Simulated and measured x-polarized far-field results. e) Simulated and measured y-polarized far-field results. f) Intensity and phase distributions of OAM +1 and −1 modes in the near-field simulations (upper panels) and measurements (lower panels). Note that the staircase effects in the experimental phase patterns are due to the measurement sampling, and cannot be smoothed out due to the phase jumps.

$$T(x, y) = A_1 \exp \left[jk \left(\sqrt{(x+d_{1x})^2 + (y+d_{1y})^2 + F^2} - F \right) \right] + A_2 \exp \left[jk \left(\sqrt{(x+d_{2x})^2 + (y+d_{2y})^2 + F^2} - F \right) \right] \quad (7)$$

where the meaning of the parameters is similar to the 1D case above.

By combining the axial and lateral cases together, two arbitrary and independent focal points can be attained in the

transmission region. Now, Equations (6) and (7) are integrated to form a more complicated condition as

$$T(x, y) = A_1 \exp \left[jk \left(\sqrt{(x+d_{1x})^2 + (y+d_{1y})^2 + F_1^2} - F_1 \right) \right] + A_2 \exp \left[jk \left(\sqrt{(x+d_{2x})^2 + (y+d_{2y})^2 + F_2^2} - F_2 \right) \right] \quad (8)$$

Table 2. Details for the synthesis of multiple equal-power vortex beams.

Polarization	OAM mode	Coding sequence	Deflection angle	Amplitude value
x-polarized	0	00000000@x	0°	0.5868
	0	33221100@x	−22.3°	0.6345
	0	01230123@x	+49.2°	0.9
y-polarized	0	00000000@y	0°	0.36
	+1	33221100@y	−22.3°	0.639
	−1	01230123@y	+49.2°	0.9

Equation (8) can be regarded as the most universal expression for a bifocal metalens, yielding an arbitrary dual-focusing response. These relationships lay the foundations for our novel polarization-reconfigurable arbitrary bifocal metalens, relying on anisotropic metasurfaces with full A – P control. In addition, they can also be extended to three or more focusing spots by superposing additional metalens patterns.

To illustrate the arbitrary dual-focusing response, we designed several samples. First, we consider a 1D bifocal metalens with polarization-reconfigurable axial and lateral response by relying on a metasurface sample including 31×31 meta-atoms. In this example, both functionalities are designed to work at 10 GHz. For the x -polarized axial case, we set

$F_1 = 120$ mm and $F_2 = 250$ mm, whereas for the y -polarized lateral case, we set $d_1 = -40$ mm and $d_2 = 40$ mm with focal length $F = 150$ mm. The calculated 1D amplitude and phase profiles for the two cases are shown in Figure 4a,c respectively, in which the maximum amplitude is converted to 0.9 to account for the maximum transmission attainable. The blue curves represent the theoretically calculated amplitude and phase profiles, whereas the red markers are the actual values for the 31 rows of meta-atoms. Figure 4b,d shows the simulated results, with magnified details at the focal planes displayed in the insets. Two focusing spots with different focal lengths and different offset distances can be observed in the x – z and y – z planes, respectively, in agreement with the design specifications. We also carry out near-field measurements for further validation of the dual-focusing response, as illustrated in Figure S6 in the Supporting Information. The fabricated sample is shown in Figure 4e. Although, in view of some experimental restrictions, we only measure the intensity distribution in the focal planes, these results provide sufficient evidence of the focusing capabilities. Figure 4f,g illustrates the measured results for the x -polarized axial dual-focusing response at the planes $z = 120$ mm and $z = 250$ mm, respectively. Both show a clear focusing effect in the 1D case. Moreover, in Figure 4h, two focusing traces are observed at the predesigned focal plane $z = 150$ mm, in good agreement with the theoretical and numerical predictions.

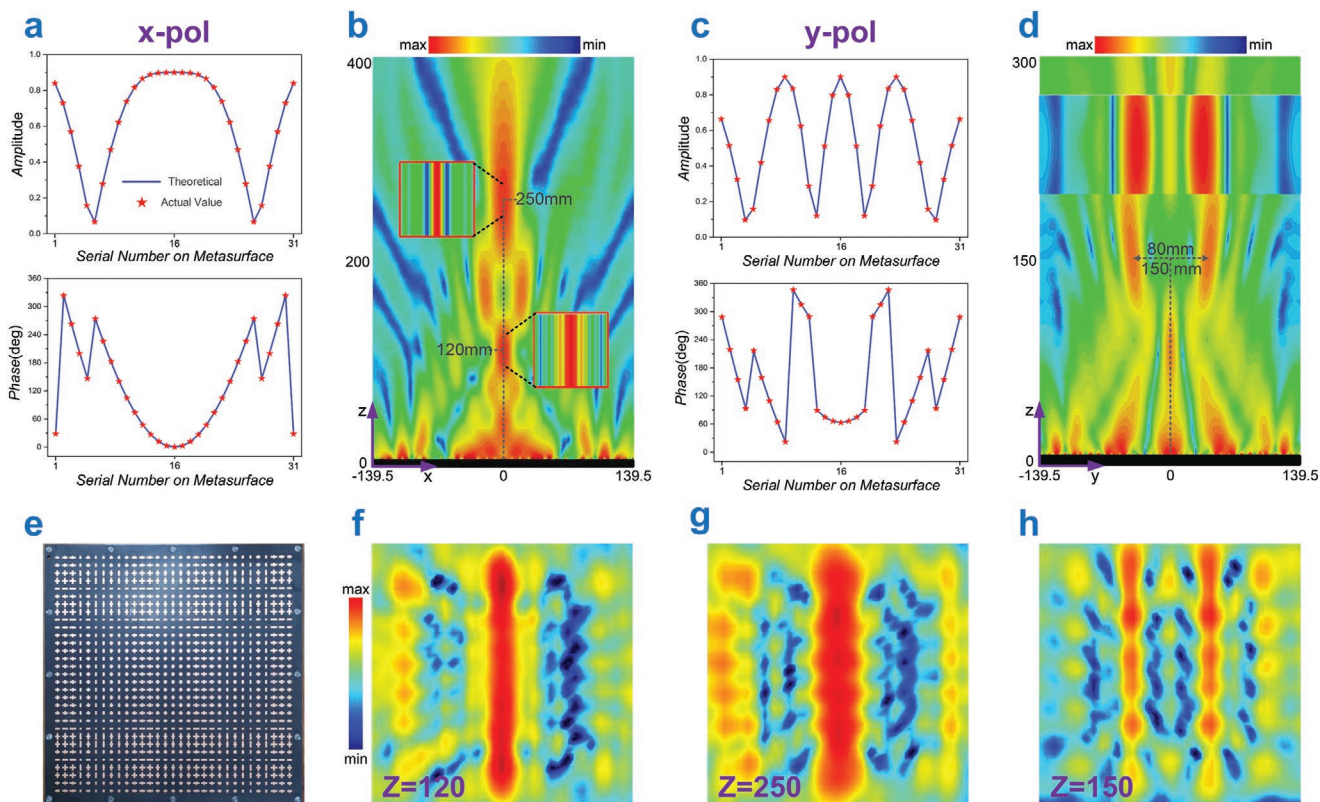


Figure 4. a) Amplitude and phase profiles for the 1D x -polarized axial bifocal metalens. b) Simulated near-field intensity distribution in the x – z plane; the insets display magnified details at the focal planes $z = 120$ mm and $z = 250$ mm. c) Amplitude and phase profiles for the 1D y -polarized lateral bifocal metalens. d) Simulated near-field intensity distribution in the y – z plane; the inset displays magnified details at the focal plane $z = 150$ mm. e) Photograph of the fabricated prototype. f,g) Measured near-field intensity distributions of the x -polarized axial dual-focusing response at the focal planes $z = 120$ mm and $z = 250$ mm, respectively. h) Measured near-field intensity distribution of the y -polarized axial dual-focusing response at the focal plane $z = 150$ mm.

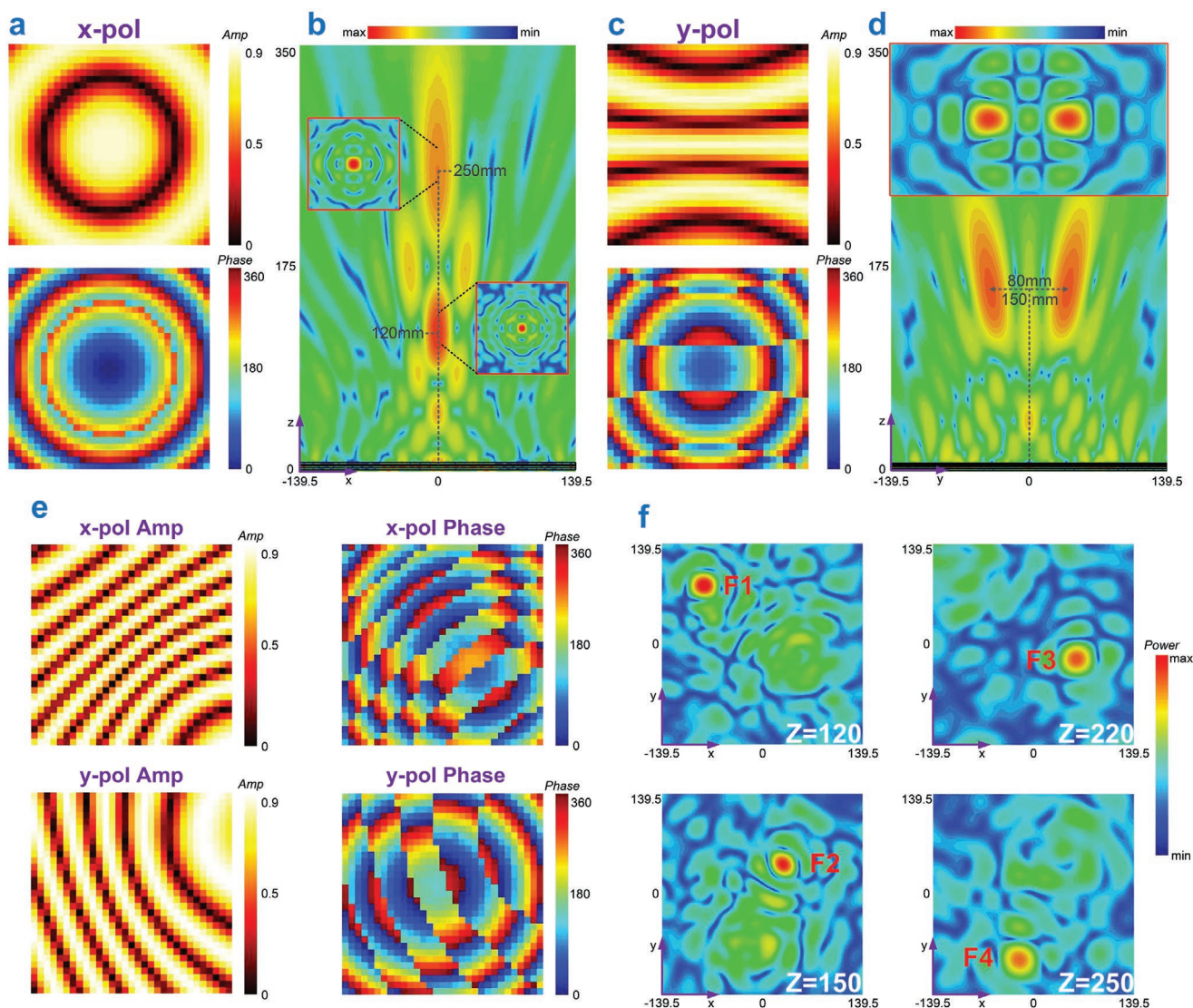


Figure 5. a) Amplitude and phase distributions for the 2D x-polarized axial bifocal metalens. b) Simulated near-field intensity distribution in the x - z plane; the insets display magnified details at the focal planes $z = 120$ mm and $z = 150$ mm. c) Amplitude and phase distributions for the 2D y-polarized lateral bifocal metalens. d) Simulated near-field intensity distribution in the y - z plane; the inset displays magnified details at the focal plane $z = 150$ mm. e) Amplitude and phase distributions for the arbitrary four-focal metalens obtained by integrating the x-polarized and y-polarized cases of 2D arbitrary bifocal metalenses. f) Simulated near-field intensity distributions at the four predesigned focal planes $z = 120$ mm, $z = 150$ mm, $z = 220$ mm, and $z = 250$ mm, showing four focal points in different quadrants.

We can also design a 2D polarization-reconfigurable arbitrary bi-focal metalens, according to Equations (6) and (7). The amplitude and phase distributions for the designed 2D axial (x-polarized) and lateral (y-polarized) dual-focusing responses are shown in Figure 5a,c, respectively, while the meta-atoms arrangement is shown in Figure S7a,b in the Supporting Information. To demonstrate the multifrequency operability, the working frequency is now selected as 12 GHz. From the simulated results, shown in Figure 5b,d, we observe the focusing effects in the two predesigned orthogonal planes, similar as the 1D case. In this case, the intensity distributions at the focal planes are no longer extended but point-shaped.

As a final example, we implement a fairly complicated design with four arbitrary focusing points at 12 GHz, by integrating

two arbitrary bifocal metalens according to Equation (8), while assuming x - and y -polarized excitations simultaneously. The parameters for the x-polarized design are $F_1 = 120$ mm, $F_3 = 220$ mm, $d_{1x} = -80$ mm, $d_{1y} = 80$ mm, $d_{3x} = 60$ mm, and $d_{3y} = -20$ mm. For the y-polarized case, the corresponding parameters are $F_2 = 150$ mm, $F_4 = 250$ mm, $d_{2x} = 40$ mm, $d_{2y} = 30$ mm, $d_{4x} = -20$ mm, and $d_{4y} = -90$ mm. The resulting 2D amplitude and phase distributions are shown in Figure 5e. The final layout for this design is shown in Figure S7c,d in the Supporting Information. From the simulated results shown in Figure 5f, we observe the expected four focal spots in the different quadrants and with different focal lengths.

The above illustrated results demonstrate that the proposed anisotropic A - P controllable metasurface is capable to

achieve advanced multifocusing responses, which are also polarization-reconfigurable.

We have proposed an anisotropic design of transmitting metasurfaces which allows, for the first time, independent and simultaneous control of copolarized phase and amplitude responses to two linear, orthogonal polarizations. By changing the geometrical parameters of our proposed meta-atom, the transmission amplitude and phase responses to x - and y -polarized fields can be fully controlled without introducing cross-polarized responses. Moreover, via suitably changing the variation ranges, the operational frequency can be tuned over a wide range, thereby paving the way to the development of broadband programmable metasurfaces.

This innovative design enables the synthesis of advanced field manipulations and functionalities such as the radiation of multiple equal-power vortex beams and polarization-reconfigurable arbitrary bifocal metalenses. Simulated and experimental results confirm the effectiveness of our proposed approach and demonstrate the enhancements by comparison with existing isotropic A - P controllable metasurfaces. Current and future research is aimed at implementing “programmable” responses, and well as exploring possible applications to radar and communication systems. Extensions of the proposed concept to millimeter-wave and terahertz frequencies are also of great interest.

Experimental Section

For all numerical simulations, the commercial software CST Microwave Studio (see <https://www.3ds.com/products-services/simulia/products/cst-studio-suite/>) is relied on. For the study in Figure 4, a waveguide port was utilized as a feed, at a distance of 170 mm from the metasurface. For the study in Figure 5, a normally incident plane-wave illumination was assumed.

The prototypes were fabricated through standard printed circuit board technology. Around the useful area, an additional part was utilized as a supporting structure, with several plastic screws inserted to tighten the multiple layers. Details on the near- and far-field measurement setups are provided in the Supporting Information.

Supporting Information

Supporting Information is available from the Wiley Online Library or from the author.

Acknowledgements

This project is supported by the National Key Research and Development Program of China (2017YFA0700201, 2017YFA0700202, 2017YFA0700203), the National Natural Science Foundation of China (61631007, 61731010, 61735010, 61722106, 61701107, 61701108), the Fund for International Cooperation and Exchange of the National Natural Science Foundation of China (61761136007), the 111 Project (111-2-05), Fundamental Research Funds for the Central Universities and Postgraduate Research & Practice Innovation Program of Jiangsu Province (KYCX17_0092), and the Scientific Research Foundation of Graduate School of Southeast University (YBJJ-1815). V.G. acknowledges partial support from the FRA Program of the University of Sannio and by the Italian Ministry of Education, University and Research through the PON Program (PM³ project).

Conflict of Interest

The authors declare no conflict of interest.

Keywords

amplitude and phase control, anisotropic metasurfaces, arbitrary bifocal metalenses, equal-power vortex beams, polarization-reconfigurable

Received: December 19, 2019

Revised: February 28, 2020

Published online:

- [1] C. L. Holloway, E. F. Kuester, J. A. Gordon, J. O'Hara, J. Booth, D. R. Smith, *IEEE Antennas Propag. Mag.* **2012**, 54, 10.
- [2] H. T. Chen, A. J. Taylor, N. Yu, *Rep. Prog. Phys.* **2016**, 79, 076401.
- [3] D. Sievenpiper, L. Zhang, L. R. F. J. Broas, N. G. Alexopolous, E. Yablonovitch, *IEEE Trans. Microwave Theory Technol.* **1999**, 47, 2059.
- [4] E. F. Kuester, M. A. Mohamed, M. Piket-May, C. L. Holloway, *IEEE Trans. Antennas Propag.* **2003**, 51, 2641.
- [5] R. E. Collin, *Field Theory of Guided Waves*, McGraw-Hill, New York **1960**.
- [6] N. F. Yu, P. Genevet, M. A. Kats, F. Aieta, J. P. Tetienne, F. Capasso, Z. Gaburro, *Science* **2011**, 334, 333.
- [7] J. Zhao, Q. Cheng, J. Chen, M. Q. Qi, W. X. Jiang, T. J. Cui, *New J. Phys.* **2013**, 15, 043049.
- [8] S. Sun, K. Y. Yang, C. M. Wang, T. K. Juan, W. T. Chen, C. Y. Liao, Q. He, S. Xiao, W. T. Kung, G. Y. Guo, L. Zhou, D. P. Tsai, *Nano Lett.* **2012**, 12, 6223.
- [9] E. Karimi, S. A. Schulz, I. D. Leon, H. Qassim, J. Upham, R. W. Boyd, *Light: Sci. Appl.* **2014**, 3, e167.
- [10] C. Pfeiffer, A. Grbic, *Phys. Rev. Lett.* **2013**, 110, 197401.
- [11] K. Chen, Y. Feng, F. Monticone, J. Zhao, B. Zhu, T. Jiang, L. Zhang, Y. Kim, X. Ding, S. Zhang, A. Alù, C.-W. Qiu, *Adv. Mater.* **2017**, 29, 1606422.
- [12] S. L. Sun, Q. He, S. Xiao, Q. Xu, X. Li, L. Zhou, *Nat. Mater.* **2012**, 11, 426.
- [13] X. Wan, X. Shen, Y. Luo, T. J. Cui, *Laser Photonics Rev.* **2014**, 8, 757.
- [14] A. Arbabi, Y. Horie, M. Bagheri, A. Faraon, *Nat. Nanotechnol.* **2015**, 10, 937.
- [15] K. Ou, G. Li, T. Li, H. Yang, F. Yu, J. Chen, Z. Zhao, G. Cao, X. Chen, W. Lu, *Nanoscale* **2018**, 10, 19154.
- [16] Z. Li, W. Wang, D. Rosenmann, D. A. Czaplewski, X. Yang, J. Gao, *Opt. Express* **2016**, 24, 20472.
- [17] G. Valerio, F. Ghasemifard, Z. Sipus, O. Quevedo-Teruel, *IEEE Trans. Microwave Theory Technol.* **2018**, 66, 3210.
- [18] N. M. Estakhri, A. Alù, *Phys. Rev. X* **2016**, 6, 041008.
- [19] V. S. Asadchy, M. Albooyeh, S. N. Tsvetkova, A. Díaz-Rubio, Y. Ra'di, S. A. Tretyakov, *Phys. Rev. B* **2016**, 94, 075142.
- [20] S. N. Tsvetkova, D.-H. Kwon, A. Díaz-Rubio, S. A. Tretyakov, *Phys. Rev. B* **2018**, 97, 115447.
- [21] T. J. Cui, M. Q. Qi, X. Wan, J. Zhao, Q. Cheng, *Light: Sci. Appl.* **2014**, 3, e218.
- [22] K. Fan, J. Y. Suen, X. Liu, W. J. Padilla, *Optica* **2017**, 4, 601.
- [23] P. C. Wu, W. Zhu, Z. X. Shen, P. H. J. Chong, W. Ser, D. P. Tsai, A. Q. Liu, *Adv. Opt. Mater.* **2017**, 5, 1600938.
- [24] H. Yang, G. Li, X. Su, G. Cao, Z. Zhao, F. Yu, X. Chen, W. Lu, *Opt. Express* **2017**, 25, 16907.
- [25] A. Pors, M. G. Nielsen, R. L. Eriksen, S. I. Bozhevolnyi, *Nano Lett.* **2013**, 13, 829.

- [26] H. Yang, G. Li, G. Cao, Z. Zhao, F. Yu, X. Chen, W. Lu, *Opt. Lett.* **2017**, 42, 3996.
- [27] X. Ni, A. V. Kildishev, V. M. Shalae, *Nat. Commun.* **2013**, 4, 2807.
- [28] G. Zheng, H. Mühlenbernd, M. Kenney, G. Li, T. Zentgraf, S. Zhang, *Nat. Nanotechnol.* **2015**, 10, 308.
- [29] G. Li, B. P. Clarke, J. So, K. F. MacDonald, N. I. Zheludev, *Nat. Commun.* **2016**, 7, 13705.
- [30] H. F. Ma, T. J. Cui, *Nat. Commun.* **2010**, 1, 124.
- [31] N. Kundtz, D. R. Smith, *Nat. Mater.* **2010**, 9, 129.
- [32] L. Liu, X. Zhang, M. Kenney, X. Su, N. Xu, C. Ouyang, Y. Shi, J. Han, W. Zhang, S. Z, *Adv. Mater.* **2014**, 26, 5031.
- [33] J. Ding, S. An, B. Zheng, H. Zhang, *Adv. Opt. Mater.* **2017**, 5, 1700079.
- [34] H. X. Xu, G. Hu, L. Han, M. Jiang, Y. Huang, Y. Li, X. Yang, X. Ling, L. Chen, J. Zhao, C. W. Qiu, *Adv. Opt. Mater.* **2019**, 7, 1801479.
- [35] H. X. Xu, G. Hu, Y. Li, L. Han, J. Zhao, Y. Sun, F. Yuan, G. M. Wang, Z. H. Jiang, X. Ling, T. J. Cui, C. W. Qiu, *Light: Sci. Appl.* **2019**, 8, 3.
- [36] L. Bao, R. Y. Wu, X. Fu, Q. Ma, G. D. Bai, J. Mu, R. Jiang, T. J. Cui, *IEEE Trans. Antennas Propag.* **2019**, 67, 6680.
- [37] L. Bao, Q. Ma, G. D. Bai, H. B. Jing, R. Y. Wu, X. J. Fu, C. Yang, J. W. Wu, T. J. Cui, *Appl. Phys. Lett.* **2018**, 113, 063502.
- [38] X. Wan, S. L. Jia, T. J. Cui, Y. J. Zhao, *Sci. Rep.* **2016**, 6, 25639.
- [39] R. Y. Wu, L. Zhang, L. Bao, L. W. Wu, Q. Ma, G. D. Bai, H. T. Wu, T. J. Cui, *Adv. Opt. Mater.* **2019**, 7, 1801429.
- [40] R. Y. Wu, Y. B. Li, W. Wu, C. B. Shi, T. J. Cui, *IEEE Trans. Antennas Propag.* **2017**, 65, 3481.
- [41] R. Y. Wu, C. B. Shi, S. Liu, W. Wu, T. J. Cui, *Adv. Opt. Mater.* **2018**, 6, 1701236.
- [42] H. Rajabalipanah, A. Abdolali, J. Shabanpour, A. Momeni, A. Cheldavi, *ACS Omega* **2019**, 4, 14340.
- [43] Y. Li, X. Li, L. Chen, M. Pu, J. Jin, M. Hong, X. Luo, *Adv. Opt. Mater.* **2017**, 5, 1600502.
- [44] S. Yu, L. Li, G. Shi, C. Zhu, Y. Shi, *Appl. Phys. Lett.* **2016**, 108, 241901.
- [45] X. Chen, M. Chen, M. Q. Mehmood, D. Wen, F. Yue, C. W. Qiu, S. Zhang, *Adv. Opt. Mater.* **2015**, 3, 1201.
- [46] R. Li, Z. Guo, W. Wang, J. Zhang, K. Zhou, J. Liu, S. Qu, S. Liu, J. Gao, *Photon. Res.* **2015**, 3, 252.
- [47] S. Liu, T. J. Cui, L. Zhang, Q. Xu, Q. Wang, X. Wan, J. Q. Gu, W. X. Tang, M. Q. Qi, J. G. Han, W. L. Zhang, X. Y. Zhou, Q. Cheng, *Adv. Sci.* **2016**, 3, 1600156.